

Computational analysis for selectivity of histone deacetylase inhibitor by replica-exchange umbrella sampling molecular dynamics simulations

Shuichiro Tsukamoto, Yoshitake Sakae, Yukihiro Itoh, Takayoshi Suzuki, and Yuko Okamoto

Citation: *J. Chem. Phys.* **148**, 125102 (2018); doi: 10.1063/1.5019209

View online: <https://doi.org/10.1063/1.5019209>

View Table of Contents: <http://aip.scitation.org/toc/jcp/148/12>

Published by the [American Institute of Physics](#)

Articles you may be interested in

[Quantum chemical replica-exchange umbrella sampling molecular dynamics simulations reveal the formation mechanism of iron phthalocyanine from iron and phthalonitrile](#)

The Journal of Chemical Physics **149**, 072332 (2018); 10.1063/1.5026956

[Multidimensional replica-exchange method for free-energy calculations](#)

The Journal of Chemical Physics **113**, 6042 (2000); 10.1063/1.1308516

[Transition path sampling of rare events by shooting from the top](#)

The Journal of Chemical Physics **147**, 152716 (2017); 10.1063/1.4997378

[Flexible selection of the solute region in replica exchange with solute tempering: Application to protein-folding simulations](#)

The Journal of Chemical Physics **149**, 072304 (2018); 10.1063/1.5016222

[How proteins modify water dynamics](#)

The Journal of Chemical Physics **148**, 215103 (2018); 10.1063/1.5026861

[Refining Markov state models for conformational dynamics using ensemble-averaged data and time-series trajectories](#)

The Journal of Chemical Physics **148**, 241731 (2018); 10.1063/1.5019750

PHYSICS TODAY

WHITEPAPERS

ADVANCED LIGHT CURE ADHESIVES

Take a closer look at what these environmentally friendly adhesive systems can do

READ NOW

PRESENTED BY
 MASTERBOND
ADHESIVES | SEALANTS | COATINGS

Computational analysis for selectivity of histone deacetylase inhibitor by replica-exchange umbrella sampling molecular dynamics simulations

Shuichiro Tsukamoto,^{1,2} Yoshitake Sakae,¹ Yukihiro Itoh,^{2,3} Takayoshi Suzuki,^{2,3} and Yuko Okamoto^{1,2,4,5,6}

¹Department of Physics, Graduate School of Science, Nagoya University, Nagoya, Aichi 464-8602, Japan

²Core Research for Evolutional Science and Technology (CREST), Japan Science and Technology Agency (JST), Kawaguchi, Saitama 332-0012, Japan

³Graduate School of Medical Science, Kyoto Prefectural University of Medicine, Kyoto, Kyoto 606-0823, Japan

⁴Structural Biology Research Center, Graduate School of Science, Nagoya University, Nagoya, Aichi 464-8602, Japan

⁵Center for Computational Science, Graduate School of Engineering, Nagoya University, Nagoya, Aichi 464-8603, Japan

⁶Information Technology Center, Nagoya University, Nagoya, Aichi 464-8601, Japan

(Received 12 December 2017; accepted 5 March 2018; published online 30 March 2018)

We performed protein-ligand docking simulations with a ligand T247, which has been reported as a selective inhibitor of a histone deacetylase HDAC3, by the replica-exchange umbrella sampling method in order to estimate the free energy profiles along ligand docking pathways of HDAC3-T247 and HDAC2-T247 systems. The simulation results showed that the docked state of the HDAC3-T247 system is more stable than that of the HDAC2-T247 system although the amino-acid sequences and structures of HDAC3 and HDAC2 are very similar. By comparing structures obtained from the simulations of both systems, we found the difference between structures of hydrophobic residues at the entrance of the catalytic site. Moreover, we performed conventional molecular dynamics simulations of HDAC3 and HDAC2 systems without T247, and the results also showed the same difference of the hydrophobic structures. Therefore, we consider that this hydrophobic structure contributes to the stabilization of the docked state of the HDAC3-T247 system. Furthermore, we show that Tyr209, which is one of the hydrophobic residues in HDAC2, plays a key role in the instability from the simulation results of a mutated-HDAC2 system. *Published by AIP Publishing.* <https://doi.org/10.1063/1.5019209>

INTRODUCTION

Histone deacetylases (HDACs) regulate the gene transcription by catalyzing deacetylation of acetylated lysines on histone tails in eukaryotic cells.^{1,2} The acetylation levels of histones are related to chromatin remodeling. For example, deacetylation by HDACs leads to gene silencing. On the other hand, histone acetylation activates gene transcription. These are representative epigenetic control for gene expression. The activities of HDACs also have correlation with some diseases such as cancer and neurological diseases. Therefore, HDACs are important targets of the drug design for these diseases.^{3–5}

There are 18 isozymes of mammalian HDACs. These isozymes are divided into four classes by homology of the amino-acid sequence.⁶ Thus, the structures of the HDACs which belong to the same class are very similar (see Fig. 1). There have been many efforts to discover isozyme selective HDAC inhibitors because high isozyme selectivity is expected to be effective for the discovery of drugs with low side-effects.^{8–11} T247 is reported as an isozyme selective inhibitor¹¹ (see Fig. 2). T247 can inhibit HDAC3 strongly but scarcely inhibit other HDACs even those in the same class as HDAC3. The purpose of this study is to elucidate the mechanism

of isozyme selectivity at the atomic level by generalized-ensemble molecular dynamics (MD) simulations (for a review, see, e.g., Ref. 12).

In order to verify the selectivity of T247, we calculated the free energy profiles along the ligand binding pathway of two systems, those of HDAC3 and HDAC2, as the potential of mean force (PMF) about the distance between zinc binding groups of T247 and ligand binding sites of HDACs and compared them. A zinc binding group is the region which is expected to approach the catalytic sites of HDACs. One of these two systems consists of HDAC3 and T247 (which is referred to as the HDAC3-T247 system henceforth) and the other system consists of HDAC2 and T247 (which is referred to as the HDAC2-T247 system henceforth). HDAC3 is a target enzyme of T247. HDAC2 is selected to compare with HDAC3 because both of them are the members of class I HDACs and have very similar amino-acid sequences and three-dimensional structures especially around the catalytic site. PMF shows the relative stability of the states which have the specific reaction coordinate. The smaller value of PMF the state has, the more stable it is. In order to obtain the PMF, we applied the replica-exchange umbrella sampling (REUS)¹³ method to molecular dynamics (MD) simulations (for the applications of molecular simulations to ligand docking, see, e.g., Refs. 14–20).

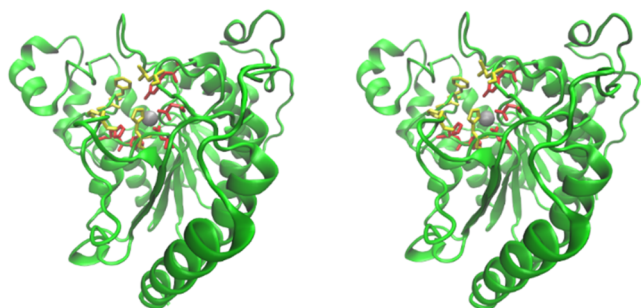


FIG. 1. Structures of HDAC3 (left) and HDAC2 (right). Red stick models indicate the residues around the catalytic site. Yellow stick models correspond to hydrophobic residues about which are discussed in the main text. Both HDACs belong to class I. The figures were created with VMD.⁷

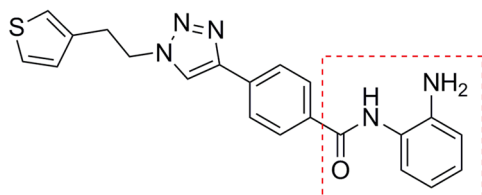


FIG. 2. Selective HDAC inhibitor T247. This ligand inhibits the activities of only HDAC3. The benzamide region, which is referred to as the zinc binding group and enclosed by the red rectangle with dashed lines, is expected to bind to the catalytic site of HDACs.

The REUS method is an efficient conformational sampling technique to sample along a reaction coordinate across energy barriers.

METHODS AND SIMULATION DETAILS

We explain the REUS method briefly. In this method, we prepare M non-interacting replicas of the original system which have umbrella potentials $V_m(q)$, ($m = 1, 2, \dots, M$), where q are the atomic coordinates of each replica. When the i th replica has the m th umbrella potential $V_m(q)$, the Hamiltonian of this replica is given by

$$H_m(q^{[i]}, p^{[i]}) = K(p^{[i]}) + E_0(q^{[i]}) + V_m(q^{[i]}), \quad (1)$$

where $K(p^{[i]})$ and $E_0(q^{[i]})$ are the kinetic energy and original, non-biased potential energy of the i th replica, respectively, and $p^{[i]}$ are the momenta of the replica. In this study, each umbrella potential was defined by the following harmonic potential:

$$V_m(q) = k_m(\xi(q) - d_m)^2, \quad (2)$$

where ξ is a reaction coordinate, d_m is the mid-point distance, and k_m is the strength of the restraint. In the REUS method, we try to exchange a pair of the replicas with “neighboring” umbrella potentials during the simulations. For example, the exchange of the i th replica with umbrella potential V_m and the j th replica with V_n gives

$$\begin{aligned} X &= \left\{ \dots, x_m^{[i]}, \dots, x_n^{[j]}, \dots \right\} \rightarrow \\ X' &= \left\{ \dots, x_m^{[j]}, \dots, x_n^{[i]}, \dots \right\}, \end{aligned} \quad (3)$$

where $x_m^{[i]} = (q^{[i]}, p^{[i]})_m$ is the state of the i th replica with V_m and X stands for the state of the whole system. The exchange probability $\omega(x_m^{[i]} | x_n^{[j]})$ is given by the Metropolis criterion,

$$\omega(x_m^{[i]} | x_n^{[j]}) = \begin{cases} 1 & (\Delta \leq 0) \\ \exp(-\Delta) & (\Delta > 0) \end{cases}, \quad (4)$$

$$\begin{aligned} \Delta &= \beta \left(V_m(\xi(q^{[j]})) + V_n(\xi(q^{[i]})) \right. \\ &\quad \left. - V_m(\xi(q^{[i]}) - V_n(\xi(q^{[j]})) \right). \end{aligned} \quad (5)$$

Each replica can move widely along the reaction coordinate by replica exchange. Thus, we can sample conformations effectively along the reaction coordinate.

To define reaction coordinates, we selected five residues around the ligand-binding sites of each HDAC (Trp129, Leu133, His135, Cys256, and Ala258 for HDAC3 and His145, Ile178, Leu264, Leu303, and Gly306 for HDAC2) and defined the reaction coordinates as distances between the geometric center with respect to the heavy atoms of the main chain of the five residues and the geometric center with respect to the heavy atoms of T247's zinc-binding group. Thus, the reaction coordinates are comparable to the distance between the ligand-binding site of HDACs and T247 zinc binding group. The range of the restraining potential along the reaction coordinate was defined as from 3.0 Å to 22.0 Å for the HDAC3-T247 system and from 5.0 Å to 24.0 Å for the HDAC2-T247 system and the midpoints of harmonic restraints were distributed in this range. The details about the parameters of the umbrella potentials are shown in Table I.

For our MD simulations, we prepared two systems (HDAC3-T247 system and HDAC2-T247 system). Initial protein structures of these systems were taken from the Protein Data Bank (PDB). The PDB codes were 4a69²¹ for HDAC3 and 3max²² for HDAC2. Chain A of both structures was used for simulations, and the molecules, except the chain A protein and water molecules around the chain A protein, were removed. The AMBER ff99SB force field²³ was used for proteins, and the TIP3P water model²⁴ was used for the solvent. The CM Lennard-Jones parameter sets for the TIP3P water model of divalent metal cations proposed in Ref. 25 were adopted for Zn²⁺ and Ca²⁺ (the charges for these ions were thus +2). Similar treatment of the force fields including metals can also be found in Refs. 26 and 27. Charge parameters of the T247 were determined by the Restrained Electrostatic Potential (RESP) method,²⁸ and the general amber force field (GAFF)²⁹ was applied to the force field parameters of T247. The docked structures predicted by Molegro Virtual Docker (MVD) were used for initial ligand structures. T247 was fitted in the catalytic site of each HDAC in both predicted docked structures. Both systems were solvated in truncated octahedron TIP3P water boxes with sides at least 12.0 Å from the protein surface and periodic boundary conditions were imposed on both systems. The numbers of water molecules were 11 700 for the HDAC3-T247 system and 11 562 for the HDAC2-T247 system, respectively.

Before our MD simulations, we performed relaxation simulations of the two systems. At first, 5000-step energy

TABLE I. Parameters of the umbrella potentials in Eq. (2) for the HDAC3-T247 system (upper) and HDAC2-T247 system (lower).^a

d_m (Å)	k_m ($\frac{\text{kcal}}{\text{mol Å}^2}$)	d_m (Å)	k_m ($\frac{\text{kcal}}{\text{mol Å}^2}$)	d_m (Å)	k_m ($\frac{\text{kcal}}{\text{mol Å}^2}$)	d_m (Å)	k_m ($\frac{\text{kcal}}{\text{mol Å}^2}$)
3.0	1.0	7.0	1.0	11.0	1.0	15.0	1.0
3.5	1.0	7.5	1.0	11.5	1.0	16.0	0.5
4.0	1.0	8.0	1.0	12.0	1.0	17.0	0.5
4.5	1.0	8.5	1.0	12.5	1.0	18.0	0.5
5.0	1.0	9.0	1.0	13.0	1.0	19.0	0.5
5.5	1.0	9.5	1.0	13.5	1.0	20.0	0.5
6.0	1.0	10.0	1.0	14.0	1.0	21.0	0.5
6.5	1.0	10.5	1.0	14.5	1.0	21.0	0.5
d_m (Å)	k_m ($\frac{\text{kcal}}{\text{mol Å}^2}$)	d_m (Å)	k_m ($\frac{\text{kcal}}{\text{mol Å}^2}$)	d_m (Å)	k_m ($\frac{\text{kcal}}{\text{mol Å}^2}$)	d_m (Å)	k_m ($\frac{\text{kcal}}{\text{mol Å}^2}$)
5.0	1.0	9.0	1.0	13.0	1.0	17.0	1.0
5.5	1.0	9.5	1.0	13.5	1.0	18.0	0.5
6.0	1.0	10.0	1.0	14.0	1.0	19.0	0.5
6.5	1.0	10.5	1.0	14.5	1.0	20.0	0.5
7.0	1.0	11.0	1.0	15.0	1.0	21.0	0.5
7.5	1.0	11.5	1.0	15.5	1.0	22.0	0.5
8.0	1.0	12.0	1.0	16.0	1.0	23.0	0.5
8.5	1.0	12.5	1.0	16.5	1.0	24.0	0.5

^aThe lowest d_m values are defined as the points that are sufficiently small by considering steric effects. The highest values of d_m values are defined as the points in which the distances between the ligands and the binding sites of proteins are sufficiently large.

minimization with restraints on heavy atoms was done. We then performed 7000-step energy minimization without the restraints. In the energy minimizations, the steepest descent method was used for the first 2000 (2500 for the second minimization) steps and the conjugate gradient method was used for the rest. For each system, we then performed a heating MD simulation for 150.0 ps from 0.0 K to 300.0 K and an isothermal-isobaric MD simulation for 5.0 ns. After the relaxation, we performed a targeted MD simulation to pull out the T247 from the catalytic site in order to make the initial structures of REUS-MD simulations independent of the MVD predictions. Finally, we performed another targeted MD to pull T247 back so that the ligand may stay around the mid-point distances of each umbrella potential. We adopted these structures as the initial structures for the REUS-MD simulations.

After the above preparations, we performed the REUS-MD simulations at 300.0 K for 120.0 ns. The data of last 80.0 ns (40.0 ns–120.0 ns) were used for data analyses. The MD simulations in the production runs and preparation runs were all canonical fixed-temperature simulations except for the 5.0 ns isothermal-isobaric simulations in the preparation runs.

Moreover, we also performed conventional MD simulations with the HDAC3, HDAC2, and Y209F HDAC2 mutant system. Unlike REUS-MD simulations, no ligands were included in these simulations. Before production simulations, we performed energy minimization, heating, and isothermal-isobaric simulations like REUS-MD simulations. After the above preparations, we performed the conventional MD simulations at 300.0 K for 150.0 ns. The MD simulations in the production runs and preparation runs were all canonical fixed-temperature simulations except for the isothermal-isobaric simulations in the preparation runs.

For all computations in this article, the Particle Mesh Ewald (PME) method³⁰ was used for electrostatic interactions. The cutoff distance for the direct space sum of PME and van der Waals interactions was 12.0 Å. The AMBER14 program package³¹ was used for all the computations. As for the MD simulations, the temperature was controlled by the Langevin thermostat³² and the pressure was controlled by the Berendsen barostat.³³ The unit time step was set to 2.0 fs. The bonds involving hydrogen atoms were constrained by the SHAKE algorithm.³⁴

RESULTS AND DISCUSSION

From the REUS-MD trajectories, we obtained PMF along the reaction coordinate by the Multistate Bennett Acceptance Ratio (MBAR) method,³⁵ which is one of the reweighting techniques (see Fig. 3). Because the reaction coordinates are defined as distances between ligand binding sites of HDACs and T247's zinc binding group, the state which has a small reaction coordinate corresponds to a docked state and that which has a large reaction coordinate means an undocked state. In the HDAC3-T247 system, the most stable state was found at 5.5 Å, and there is a relatively high free energy barrier (>4.0 kcal/mol) at 8.5 Å. Thus, the reaction coordinate of the HDAC3-T247 system can stay for a long time around 5.5 Å. This means that T247 can keep the docked state with HDAC3 long enough and have potential to inhibit the functions of HDAC3 by blocking its catalytic site. On the other hand, in the HDAC2-T247 system, the most stable state was an undocked state (the reaction coordinate is around 23.0 Å). Although the docked state of the HDAC2-T247 system exists as a metastable state (the reaction coordinate is around 12.0 Å), there is only a low energy barrier (~1.5 kcal/mol) at 14.0 Å. This result suggests that T247 is released easily from the

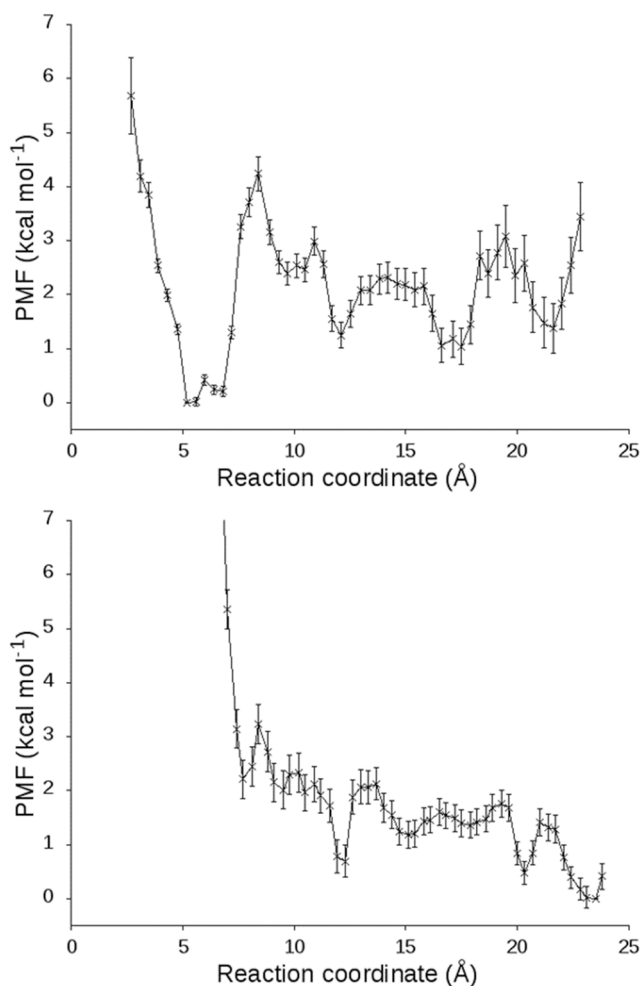


FIG. 3. PMF along the reaction coordinates of the HDAC3-T247 system (upper) and HDAC2-T247 system (lower). These were calculated from the REUS-MD trajectories by the MBAR method. The reaction coordinate is defined as the distance between the zinc binding group of T247 and catalytic site of each HDAC. Error bars are the standard deviations for each bin.

binding site and T247 scarcely inhibits HDAC2. These results qualitatively agree with the HDAC3 selectivity of T247 that was found experimentally.¹¹

We compared the docked structures of both systems to elucidate the reasons for the difference of the two PMF. We defined docked states as those where the reaction coordinate is around 5.5 Å for the HDAC3-T247 system and where the reaction coordinate is around 12.0 Å for the HDAC2-T247 system. These states were selected as the regions which have the lowest PMF in relatively small reaction coordinate regions. We show these structures in Fig. 4. In the HDAC3-T247 system, the linker region of T247 is surrounded by and in direct contact with the hydrophobic structure of six residues. This annular hydrophobic structure is placed between the catalytic site of HDAC and the outside. It consists of a histidine, a leucine, a glycine, and three phenylalanines for HDAC3 (see Fig. 4). These residues are conserved in all of the members of class I HDACs including HDAC2 (one of the phenylalanines is replaced by a tyrosine for HDAC2 and HDAC1). Because of the close contact among the six residues and T247, there are strong hydrophobic interactions among the hydrophobic linker region of T247 and the hydrophobic

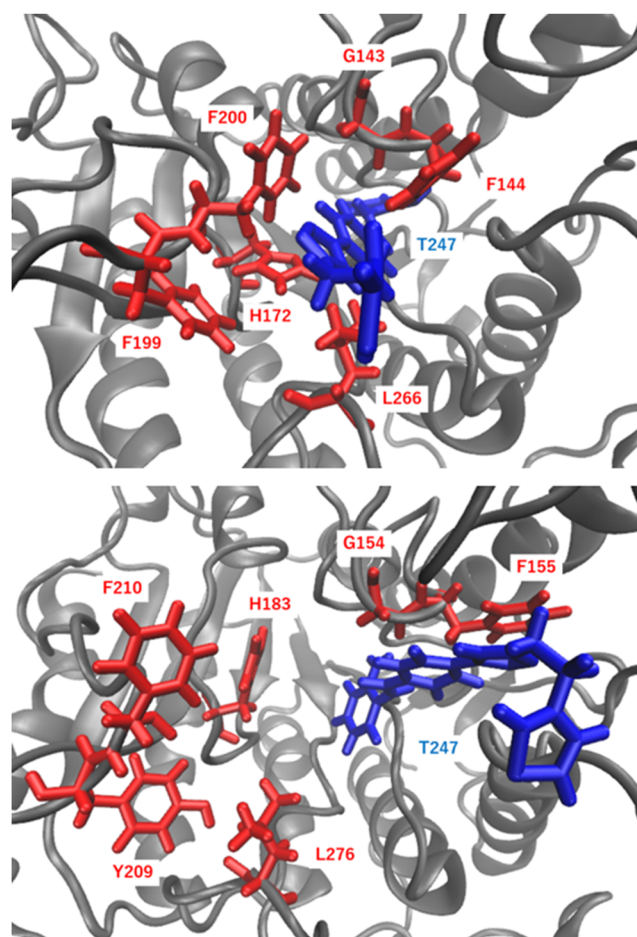


FIG. 4. Docking structures of the HDAC3-T247 system (upper) and the HDAC2-T247 system (lower). These structures were selected from those where the reaction coordinate is 5.5 Å in the HDAC3-T247 system and 12.0 Å in the HDAC2-T247 system. A blue stick model indicates T247 and red stick models correspond to the six residues which make hydrophobic structures. The figures were created with VMD.⁷

structure of HDAC3. These hydrophobic interactions make the docked structure of this system stable and suppress releasing of T247 from the catalytic site. Actually, in many docked structures of class I HDACs with other ligands similar to T247, which are uploaded in the Protein Data Bank (PDB), this hydrophobic structure takes a closed structure and makes a compact structure with the hydrophobic linker region of the ligand. On the other hand, the hydrophobic structure is open and separated from T247's linker region in the docked state of the HDAC2-T247 system. The hydrophobic interaction is weakened under such conditions. Thus, T247 is not able to stay stably in the catalytic site of HDAC2. Therefore, this structural difference leads to the difference of PMF between the HDAC3-T247 system and the HDAC2-T247 system.

In order to investigate the stability of the hydrophobic structures in the states without ligands, we performed conventional MD simulations of the HDAC3 system and the HDAC2 system in which T247 was removed. The initial structure was selected from the crystal structures downloaded from PDB. In these crystal structures, hydrophobic structures of both enzymes are closed. The radii of gyration of the hydrophobic regions of each HDAC calculated from these simulation

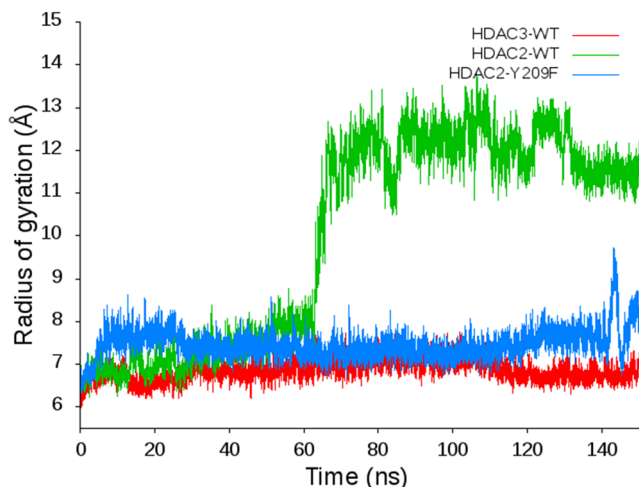


FIG. 5. Time series of the radius of gyration with respect to the six residues which are shown as red stick models in Fig. 4 for wild-type HDAC3 (red) and HDAC2 (green) and Y209F HDAC2 mutant (blue). The abscissa stands for the simulation time of conventional MD.

trajectories were plotted in Fig. 5. In the HDAC3 system, the radius of gyration kept small values (<7.0 Å). This means that the hydrophobic structure of the HDAC3 system stayed closed, even if there was no ligand in this simulation. The radius of gyration in the HDAC2 system, on the other hand, kept relatively small values (<8.0 Å) at first, but it rose up suddenly at 60.0 ns and was fluctuating around high values (~ 12.0 Å) after that. This means that the hydrophobic structure of this system was opened at this time and kept the opened structure after that. These results mean that the hydrophobic structure of HDAC2 is easy to open compared to that of HDAC3 even if there is no influence of ligands. These results are in accord with the difference of the hydrophobic structures obtained from the REUS-MD simulations.

In order to find a key residue for the reason why the hydrophobic structure of the HDAC2 system can open easily, we performed a conventional MD simulation in a mutated system. We focused on Tyr209 of HDAC2. The sequence around Tyr209 of HDAC2 and the corresponding sequence of HDAC3 are [KYGEXY209FPGTG] and [KYGNYF199FPGTG], respectively (this region of HDAC2 is shorter than that of HDAC3 by one residue and we put X for this missing site). In HDAC3, a phenylalanine residue is inserted in this region and a hydrophobic core is constructed. Because phenylalanine has strong hydrophobicity, this hydrophobic core contributes to make this inserted state stable. The tyrosine, which has less hydrophobicity than phenylalanine, is thought to be released relatively easily from the hydrophobic core. The behavior of Tyr209 has potential to affect the hydrophobic structure because this residue is the member of the hydrophobic structure and connects directly to Phe209 which is in the hydrophobic structure of HDAC2. We mutated Tyr209 of HDAC2 to phenylalanine and performed a conventional MD simulation. In Fig. 5, the radius of gyration of the mutated HDAC2 (blue curve) keeps low values during the simulation time. This result suggests that this mutation has a potential to keep the hydrophobic structure closed and that Tyr209 is the key residue that causes the instability of the hydrophobic structure. The reason for the instability of the hydrophobic

structures of the native HDAC2 may be due to the interactions of Zn^{2+} and the Tyr209 sidechain. The distance between Zn^{2+} and the oxygen of the Tyr sidechain during the simulation while the hydrophobic residues were tightly packed (before 50 ns) was indeed small (5.61–9.96 Å).

CONCLUSIONS

We performed two REUS-MD simulations and three conventional MD simulations to reproduce and analyze the HDAC3 selectivity of T247. From REUS-MD simulations, we were able to reproduce the selectivity between the HDAC3-T247 system and the HDAC2-T247 system. By comparing each docked structure, we found that the hydrophobic residues which are placed at the entrance of the catalytic site play a key role in distinguishing between HDAC3 and HDAC2. Because the difference of the hydrophobic structures was observed even if the system does not contain a ligand, the difference comes from the nature of each HDAC. This idea, thus, can be applied to other ligands. Moreover, we found that Tyr209 of HDAC2 is important for the instability of the hydrophobic structure. Finally, because HDAC1 also has a tyrosine at the same location as Tyr209 in HDAC2, we conjecture that we may be able to distinguish HDAC1 and HDAC3 by the same mechanism that we showed above.

ACKNOWLEDGMENTS

Some of the computations were performed on the supercomputers at the Institute for Molecular Science. This work was supported, in part, by the Program for Leading Graduate Schools “Integrative Graduate Education and Research in Green Natural Sciences” and by the Grant-in-Aid for Scientific Research (A) (No. JP25247071) and the Grant-in-Aid for Scientific Research on Innovative Areas “Dynamical Ordering & Integrated Functions” (No. JP25102009).

- ¹J. Taunton, C. A. Hassig, and S. L. Schreiber, *Science* **272**, 408–411 (1996).
- ²S. Y. Roth, J. M. Denu, and D. Allis, *Annu. Rev. Biochem.* **70**, 81 (2001).
- ³S. Minucci and P. G. Pelicci, *Nat. Rev. Cancer* **6**, 38 (2006).
- ⁴J. E. Bolden, M. J. Peart, and R. W. Johnstone, *Nat. Rev. Drug Discovery* **5**, 769 (2006).
- ⁵M. A. Dawson and T. Kouzarides, *Cell* **150**, 12 (2012).
- ⁶A. J. de Ruijter, A. H. van Gennip, H. N. Caron, S. Kemp, and A. B. van Kuilenburg, *Biochem. J.* **370**, 737 (2003).
- ⁷W. Humphrey, A. Dalke, and K. Schulten, *J. Mol. Graphics* **14**, 33 (1996).
- ⁸T. Suzuki, Y. Nagano, A. Kouketsu, A. Matsuura, S. Maruyama, M. Kurotaki, H. Nakagawa, and N. Miyata, *J. Med. Chem.* **48**, 1019 (2005).
- ⁹D.-F. Wang, P. Helquist, N. L. Wiech, and O. Wiest, *J. Med. Chem.* **48**, 6936 (2005).
- ¹⁰M. Bantscheff, C. Hopf, M. M. Savitski, A. Dittmann, P. Grandi, A.-M. Michon, J. Schlegl, Y. Abraham, I. Becher, G. Bergamini, M. Boesche, M. Delling, B. Dümpelfeld, D. Eberhard, C. Huthmacher, T. Mathieson, D. Poeckel, V. Reader, K. Strunk, G. Sweetman, U. Kruse, G. Neubauer, N. G. Ramsden, and G. Drewes, *Nat. Biotechnol.* **29**, 255 (2011).
- ¹¹T. Suzuki, Y. Kasuya, Y. Itoh, Y. Ota, P. Zhan, K. Asamitsu, H. Nakagawa, T. Okamoto, and N. Miyata, *PLoS One* **8**, e68669 (2013).
- ¹²A. Mitsutake, Y. Sugita, and Y. Okamoto, *Biopolymers* **60**, 96 (2001).
- ¹³Y. Sugita, A. Kitao, and Y. Okamoto, *J. Chem. Phys.* **113**, 6042 (2000).
- ¹⁴M. K. Gilson, J. A. Given, B. L. Bush, and J. A. McCammon, *Biophys. J.* **72**, 1047 (1997).
- ¹⁵E. Gallicchio, M. Lapelosa, and R. M. Levy, *J. Chem. Theory Comput.* **6**, 2961 (2010).

- ¹⁶H. Kokubo, T. Tanaka, and Y. Okamoto, *J. Comput. Chem.* **32**, 2810 (2011).
- ¹⁷J. C. Gumbart, B. Roux, and C. Chipot, *J. Chem. Theory Comput.* **9**, 794 (2013).
- ¹⁸H. Kokubo, T. Tanaka, and Y. Okamoto, *J. Comput. Chem.* **34**, 2601 (2013).
- ¹⁹Y. Okamoto, H. Kokubo, and T. Tanaka, *J. Chem. Theory Comput.* **10**, 3563 (2014).
- ²⁰L. Troussilcot, F. Guillièrre, V. Limongelli, O. Walker, and J.-M. Lancelin, *J. Am. Chem. Soc.* **137**, 1273 (2015).
- ²¹P. J. Watson, L. Fairall, G. M. Santos, and J. W. R. Schwabe, *Nature* **481**, 335 (2012).
- ²²J. C. Bressi, A. J. Jennings, R. Skene, Y. Wu, R. Melkus, R. D. Jong, S. O'Connell, C. E. Grimshaw, M. Navre, and A. R. Gangloff, *Bioorg. Med. Chem. Lett.* **20**, 3142 (2010).
- ²³V. Hornak, R. Abel, A. Okur, B. Strockbine, A. Roitberg, and C. Simmerling, *Proteins: Struct., Funct., Bioinf.* **65**, 712 (2006).
- ²⁴W. L. Jorgensen, J. Chandrasekhar, J. D. Madura, R. W. Impey, and M. L. Klein, *J. Chem. Phys.* **79**, 926 (1983).
- ²⁵P. Li, B. P. Roberts, D. K. Chakravorty, and K. M. Mertz, Jr., *J. Chem. Theory Comput.* **9**, 2733 (2013).
- ²⁶D. Chaves-Moreira, F. R. de Moraes, Í. P. Caruso, O. M. Chaim, A. Senff-Ribeiro, A. Ullah, L. S. da Silva, J. Chahine, R. K. Arni, and S. S. Veiga, *J. Cell. Biochem.* **118**, 726 (2017).
- ²⁷A. Bernini, S. Galderisi, O. Spiga, G. Bernardini, N. Niccolai, F. Manetti, and A. Santucci, *Comput. Biol. Chem.* **70**, 133 (2017).
- ²⁸C. I. Bayly, B. Cieplak, W. D. Cornell, and P. A. Kollman, *J. Phys. Chem.* **97**, 10269 (1993).
- ²⁹J. Wang, R. M. Wolf, J. W. Caldwell, P. A. Kollman, and D. A. Case, *J. Comput. Chem.* **25**, 1157 (2004).
- ³⁰T. Darken, D. York, and L. Pederson, *J. Chem. Phys.* **98**, 10089 (1993).
- ³¹D. A. Case, V. Babin, J. T. Berryman, R. M. Betz, Q. Cai, D. S. Cerutti, T. E. Cheatham III, T. A. Darden, R. E. Duke, H. Gohlke, A. W. Goetz, S. Gusarov, N. Homeyer, P. Janowski, J. Kaus, I. Kolossváry, A. Kovalenko, T. S. Lee, S. LeGrand, T. Luchko, R. Luo, B. Madej, K. M. Merz, F. Paesani, D. R. Roe, A. Roitberg, C. Sagui, R. Salomon-Ferrer, G. Seabra, C. L. Simmerling, W. Smith, J. Swails, R. C. Walker, J. Wang, R. M. Wolf, X. Wu, and P. A. Kollman, AMBER 14, University of California, San Francisco, 2014.
- ³²M. P. Allen and D. J. Tildesley, *Computer Simulation of Liquids* (Oxford University Press, New York, 1987).
- ³³H. J. C. Berendsen, J. P. M. Postma, W. F. van Gunsteren, A. DiNola, and J. R. Haak, *J. Chem. Phys.* **81**, 3684 (1984).
- ³⁴J.-P. Ryckaert, G. Ciccotti, and H. J. C. Berendsen, *J. Comput. Phys.* **23**, 327 (1997).
- ³⁵M. R. Shirts and J. D. Chodera, *J. Chem. Phys.* **129**, 124105 (2008).